Azimuth-dependent Auger neutralization of He⁺ on Ag(111) and (110) surfaces

Diego Valdés,[1,*] J. M. Blanco,[1,2] V. A. Esaulov,[3] and R. C. Monreal[1]

[1]*Departamento de Física Teórica de la Materia Condensada, Universidad Autónoma de Madrid, E-28049 Madrid, Spain*
[2]*European Space Astronomy Centre, ESAC-ESA, Ingeniería y Servicios Aeroespaciales, Spain*
[3]*Laboratoire des Collisions Atomiques et Moléculaires, Université Paris Sud, 91405 Orsay, France*

We present a detailed theoretical analysis of the role played by s and d electrons in Auger neutralization processes of He⁺ at Ag(111) and Ag(110) surfaces. We calculate crystal-lattice-site Auger neutralization rates as a function of the perpendicular distance between ions and surfaces. We find that the rate is very insensitive to the lateral position for large values of the perpendicular distance because the contribution of the delocalized s electrons dominates in this case. In contrast, the contribution of d electrons dominates at short perpendicular distances and the strong spatial localization of these electrons causes a similar strong dependence of the Auger rate with lateral position. We perform molecular dynamic simulations of scattered ion trajectories, which, used together with the Auger neutralization rates, allow us to obtain the theoretical ion fraction that we compare with our measurements. This parameter-free theory is able to reproduce the magnitude of the ion survival probability and its dependence with the azimuthal angle of incidence for both surfaces of Ag, thus showing the important role played by localized electrons in Auger neutralization of He.

PACS number(s): 79.20.Rf, 61.85.+p, 79.60.Bm

I. INTRODUCTION

Electron and energy transfer processes between an atom or molecule and a surface are extremely important for their many applications in physics and chemistry. In the case of molecules, conversion of vibrations to electron excitation in the solid has been proved very recently to be a highly efficient mechanism for energy transfer.[1,2] The two basic charge transfer mechanisms are termed in the literature resonant and Auger. Resonant processes are tunneling ones that can take place when there is an atomic level in resonance with the continuum of states of the solid. They are essentially one-electron processes that have been described abundantly in the literature using different techniques.[3–11] In contrast, Auger processes involve at least two electrons: the electron-electron interaction causes the scattering of one electron of the solid to the ion while another electron of the solid is scattered from an occupied to an unoccupied state. These processes are the only ones leading to ion neutralization of slow He⁺ ions at high-work-function surfaces, since resonant processes are not energetically allowed except at very short distances.[9] The difficulty of dealing with electron-electron interactions in a many-electron system has been the main cause why Auger processes have not been described with a comparable degree of accuracy until recently. Also, from the experimental point of view, new and relevant information about Auger neutralization processes has been obtained from measurements of ion fractions in grazing scattering of He⁺ on Ag[12–15] and Al[16,17] surfaces. Most of the calculations of the Auger neutralization rate of an ion in front of a metal surface have been performed within the jellium model,[18–23] focusing on plasmon excitation[19–21] and/or effects of the surface barrier[22,23] but corrugation effects were not included. The jellium model, being translationally invariant with respect to the surface, can only model different crystallographic faces of a solid by placing the "jellium edge" at a distance of $\frac{1}{2}d$ in front of the first atomic layer, d being the interplanar distance.[24] In this way the jellium model was also applied to explain the differences seen in the ion survival

probability of He⁺ on Ag(110) and Ag(111) surfaces in Refs. 12–14. Moreover, the role of d electrons in Auger neutralization[25] or metastable atom deexcitation[26,27] of ions and atoms at noble metal surfaces, although invoked from the experimental point of view, has been neglected theoretically.[28,29] A step forward was given in Ref. 30, where a theory for including crystal structure in the calculation of the Auger neutralization rate was developed. Very recently, the theory has been generalized to include s and d electrons and successfully applied to the calculation of the Auger neutralization rate and ion survival probability of He⁺ scattering off Ag(110) at grazing angles as a function of azimuth and incident energy in Ref. 31. In this work we present a detailed theoretical analysis of the role played by localized electrons in Auger neutralization processes which will be illustrated by comparing theory and experiment for the ion survival probability of He⁺ scattering off Ag(110) and (111) surfaces. Our theory will be expounded in Sec. II, where we show that the matrix elements for the Auger transition roughly scale with distance as the overlap integral between the wave functions of the neutralizing electron of the solid and that of the neutralized ion. This allows us to infer the range of distances between ion and surface where the different atomic orbitals of the solid are going to be important. In Sec. III we describe the experimental procedure and apparatus to measure ion fractions. Our theoretical results for the Auger neutralization rate and the ion survival probabilities will be presented in Sec. IV and compared with experiments. Finally, we present our conclusions in Sec. V.

Atomic units $e = \hbar = m = 1$ are used and distances are measured with respect to the first atomic layer throughout this paper.

II. THEORY

The starting point is the formula for the Auger neutralization rate of an ion in front of a metal surface as given in linear response theory:

$$\frac{1}{\tau}(\vec{R}_a) = 2 \sum_{\vec{k}<k_F} \int_0^\infty d\omega \int \frac{d^2\vec{q}_\parallel}{(2\pi)^2} \int_{-\infty}^\infty dz_1 \int_{-\infty}^\infty dz_2$$
$$- \mathrm{Im}\chi(\vec{q}_\parallel,\omega;z_1,z_2) V_{\vec{k}}(\vec{q}_\parallel,z_1) V_{\vec{k}}^*(\vec{q}_\parallel,z_2) \delta(\omega+E_a-\epsilon_{\vec{k}}),$$

$$(1)$$

where

$$V_{\vec{k}}(\vec{q}_\parallel,z) = \frac{2\pi}{q_\parallel} \langle \varphi_a(\vec{r}'-\vec{R}_a)|e^{i\vec{q}_\parallel\cdot\vec{\rho}'} e^{-q_\parallel|z-z'|}|\varphi_{\vec{k}}(\vec{r}')\rangle. \quad (2)$$

In Eqs. (1) and (2), φ_a is the wave function of the atomic orbital of energy E_a for an ion at the position $\vec{R}_a$ and $\varphi_{\vec{k}}$ is the wave function of a metal neutralizing electron with wave vector $\vec{k}$ and energy $\epsilon_{\vec{k}}$ below the Fermi energy. In obtaining Eq. (1), the Coulomb potential has been Fourier transformed in the coordinates parallel to the surface and the wave functions of the excited electrons have been assumed to be plane waves in these coordinates (jellium model). Thus, all possible metal excitations can be summed up, yielding the imaginary part of the surface screened susceptibility $\chi(\vec{q}_\parallel,\omega;z_1,z_2)$, which is a function of parallel momentum $\vec{q}_\parallel$ and energy ω and two electron coordinates perpendicular to the surface, z_1 and z_2. Details of the derivation of Eqs. (1) and (2) can be found in Refs. 20 and 21. In earlier works, the

wave function of the neutralizing electron appearing in Eq. (2) was also written down in the jellium model and thus the full theory was self-consistent. The shortcoming of this kind of calculation was its inability to describe surface corrugation, the jellium model being translationally invariant parallel to the surface. Moreover, the jellium model describes different materials through the one-electron radius parameter r_s and different surfaces of the same material only differ by the relative position of the edge of the positive background (the jellium edge) with respect to the first atomic plane.[24] A step forward was given in Ref. 30, where the neutralizing electron was described by a Bloch wave function written in a linear combination of atomic orbitals (LCAO) basis:

$$\varphi_{\vec{k}}(\vec{r}) = \frac{1}{\sqrt{N}} \sum_\alpha C_\alpha(\vec{k}) \sum_{\vec{R}} e^{i\vec{k}\cdot\vec{R}} \varphi_\alpha(\vec{r}-\vec{R}), \quad (3)$$

where $\varphi_\alpha(\vec{r}-\vec{R})$ is the wave function of the α orbital of the atom of the solid placed at the lattice position $\vec{R}$, N is the number of cells in the crystal, and the coefficients $C_\alpha(\vec{k})$ give rise to the band structure. Then, the matrix elements of Eq. (2) can also be expressed as linear combinations of matrix elements for atomic orbitals, which, when inserted into Eq. (1), give the following equations for the Auger neutralization rate:

$$\frac{1}{\tau}(\vec{R}_a) = 2\sum_{\alpha,\vec{R}} \sum_{\alpha',\vec{R}'} \int_0^\infty d\omega \delta(\omega+E_a-\epsilon) \rho_{\alpha\vec{R};\alpha'\vec{R}'}(\epsilon) \int \frac{d^2\vec{q}_\parallel}{(2\pi)^2} \int_{-\infty}^\infty dz_1 \int_{-\infty}^\infty dz_2 - \mathrm{Im}\chi(\vec{q}_\parallel,\omega;z_1,z_2) V_{\alpha,\vec{R}}(\vec{q}_\parallel,z_1) V_{\alpha',\vec{R}'}^*(\vec{q}_\parallel,z_2), \quad (4)$$

with

$$V_{\alpha,\vec{R}}(\vec{q}_\parallel,z) = \frac{2\pi}{q_\parallel} \langle \varphi_a(\vec{r}'-\vec{R}_a)|e^{i\vec{q}_\parallel\cdot\vec{\rho}'} e^{-q_\parallel|z-z'|}|\varphi_\alpha(\vec{r}'-\vec{R})\rangle.$$

$$(5)$$

In Eq. (4), $\rho_{\alpha\vec{R};\alpha'\vec{R}'}(\epsilon)$ are the densities of states of the unperturbed surface expressed in the basis $\{\alpha\vec{R}\}$ of localized states, as a function of energy ϵ, which has to be smaller than the Fermi energy E_F since the neutralizing electron is in an occupied state. Notice in Eq. (5) how the matrix elements depend on the product of the wave functions of the ion and the α orbital of the atom at $\vec{R}$ and, consequently, on the spatial localization of these orbitals.

The orthonormal orbitals φ_a and φ_α in Eq. (5) are obtained by means of Löwdin's prescription[32]

$$\varphi_\mu = \sum_\nu (S^{-1/2})_{\mu\nu} \psi_\nu, \quad (6)$$

ψ_ν being the initial set of atomic orbitals (AOs) for individual atoms and $S_{\mu\nu} = \langle \psi_\mu|\psi_\nu\rangle$ the overlap integral. For the case of He/Ag analyzed in this work we start with Hartree-

Fock AOs for He and Ag in the Gaussian basis of Ref. 33. We include the $1s$ orbital of He and the $5s$, $4d$, $4p$, and $4s$ orbitals of Ag; other orbitals of Ag are neglected because their overlap with He is very small. [Notice in Eq. (4) that metal electrons having energy levels below the atomic level cannot neutralize the ion. However, they should in principle be included in the construction of orthogonal orbitals.] Then, for each Ag atom at the lattice point $\vec{R}$, we apply Eq. (6) and obtain the orthonormal orbitals to be inserted into Eq. (5). This dimeric approach has already been used for analyzing different phenomena in which atoms hybridize with solid surfaces such as physisorption[34,35] and chemisorption[36,37] or resonant electron transfer between moving ions and the surface.[7–9] In our calculation, we include first, second, and third neighbors of He in the first and also in the second atomic layers. Other Ag atoms give negligible contributions. The densities of states for unreconstructed Ag surfaces have been obtained *ab initio* using the FIREBALL code of Ref. 38. Changes in densities of states due to reconstruction should not be very important for calculating the Auger neutralization rate because all the electrons below the Fermi level can participate in the process.

Coming to the calculation of the screened surface susceptibility $\chi(\vec{q}_{\parallel}, \omega; z_1, z_2)$, a consistent treatment in terms of localized orbitals cannot be hoped for at present. The evaluation of this magnitude for real metal surfaces at finite frequencies and wave vectors is still a very demanding task mainly because it requires inclusion of a large number of reciprocal wave vectors in the surface plane and, to our knowledge, only results in the quasistatic limit have been obtained for different crystallographic faces of Ag in Ref. 39. Simplified models have been proposed in which the filled d bands are modeled by a fixed lattice of point dipoles while the sp electrons are treated within the jellium model.[40,41] These models have been applied to the calculation of the relation of dispersion of surface plasmons at the different faces of Ag,[40,41] as well as to the study of the decay of image states on these surfaces.[42] In our present problem of Auger neutralization we need to evaluate χ for many values of ω and $q_{\parallel}$ (typically $0 < \omega < 0.7$ a.u. and $0 \leq q_{\parallel} \lesssim 1.5$ a.u.). Then the calculation has to be simplified by using the jellium model but with suitable modifications to take into account that either a s or a d electron can be excited in the Auger process. This is achieved by defining effective magnitudes that depend on the excitation energy ω, based on the information provided by the optical properties of Ag. The experimental results of Ref. 43 give us the number of electrons per Ag atom excited at a frequency ω. With this number we define an effective electronic density $n_{eff}(\omega)$ and an effective $r_s(\omega)$ by means of $r_s(\omega) = \left[\frac{3}{4\pi n_{eff}(\omega)}\right]^{1/3}$ and χ is then calculated for a jellium surface described by that $r_s(\omega)$. The jellium edge is canonically placed at $\frac{1}{2}d$ (Ref. 24) above the first atomic layer, d being the interplanar spacing of the different Ag surfaces, as required by charge neutrality. Surface relaxation of the Ag(110) surface amounts to a reduction in the layer spacing of $\sim 7\%$, affecting very little the results to be presented below, while atomic relaxation of the (111) and (100) surfaces is negligibly small. We have to point out that our results are sensitive to an inaccurate position of the jellium edge: when we calculate $\frac{1}{\tau}$ in Eq. (4) using atomic positions of the (110) surface but χ with the jellium edge of the (111) surface (or vice versa) our results can change by a factor of 2 and the good agreement between theory and experiment to be shown in Sec. IV is destroyed.

The main results of this work can be understood by means of a simple argument. We pointed out above that the matrix elements of Eq. (5) depend on the overlap between He and the different orbitals of Ag. Now we will show that they behave roughly like the overlap integral. Assume there is only one AO associated with each metal atom $|\psi_M\rangle$ and let $|\psi_a\rangle$ be the 1s orbital of He. Then, the Löwdin's orbitals $|\varphi_M\rangle$ and $|\varphi_a\rangle$ can be obtained, to lowest order in their overlap S_{Ma}, as

$$|\varphi_M\rangle \sim |\psi_M\rangle - \frac{1}{2} S_{Ma} |\psi_a\rangle, \tag{7}$$

$$|\varphi_a\rangle \sim |\psi_a\rangle - \frac{1}{2} S_{Ma} |\psi_M\rangle, \tag{8}$$

with $S_{Ma} \equiv \langle \psi_M | \psi_a \rangle$ the overlap integral. To the same order in S_{Ma}, Eq. (5) is then approximated as
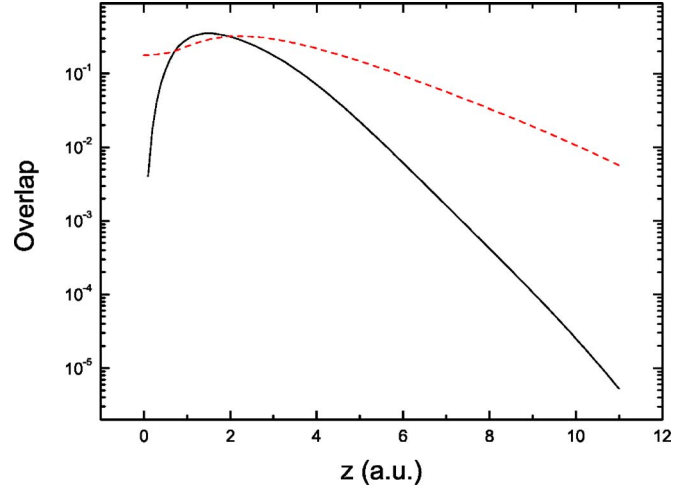

FIG. 1. (Color online) Overlap between He 1s and 5s (dashed line) and $4d_{3z^2-r^2}$ (solid line) orbitals of Ag.

$$V_M(\vec{q}_{\parallel}, z) \sim \frac{2\pi}{q_{\parallel}} \{ \langle \psi_a(\vec{r}' - \vec{R}_a) | e^{i\vec{q}_{\parallel} \cdot \vec{\rho}'} e^{-q_{\parallel}|z-z'|} | \psi_M(\vec{r}' - \vec{R}) \rangle$$
$$- \frac{1}{2} S_{Ma} [\langle \psi_a(\vec{r}' - \vec{R}_a) | e^{i\vec{q}_{\parallel} \cdot \vec{\rho}'} e^{-q_{\parallel}|z-z'|} | \psi_a(\vec{r}' - \vec{R}_a) \rangle$$
$$+ \langle \psi_M(\vec{r}' - \vec{R}) | e^{i\vec{q}_{\parallel} \cdot \vec{\rho}'} e^{-q_{\parallel}|z-z'|} | \psi_M(\vec{r}' - \vec{R}) \rangle]\}. \tag{9}$$

The first term on the right-hand side of Eq. (9) can also be approximated, for the case of ψ_a being much more localized than $|\psi_M\rangle$, as

$$\langle \psi_a(\vec{r}' - \vec{R}_a) | e^{i\vec{q}_{\parallel} \cdot \vec{\rho}'} e^{-q_{\parallel}|z-z'|} | \psi_M(\vec{r}' - \vec{R}) \rangle$$
$$\sim e^{i\vec{q}_{\parallel} \cdot \vec{R}_a} e^{-q_{\parallel}|z-z_a|} S_{Ma}. \tag{10}$$

This suggest that the full potentials of Eq. (5) should be roughly proportional to the overlap integral when $S_{Ma} \neq 0$. Equation (10) is of course invalid if $S_{Ma} = 0$, and the approximation is worse for high values of $q_{\parallel}$ since $e^{-q_{\parallel}|z-z'|}$ will also be a quickly varying function in this case.

Figure 1 shows the overlap integral between the 1s orbital of He and the 5s and $4d_{3z^2-r^2}$ orbitals of Ag. Only electrons in these orbitals can neutralize He and have nonzero overlap with it. Notice that the overlap of He with both orbitals of Ag is about the same for distances between 1 and 2 a.u. and the overlap with the 5s orbital is only a factor of 3 larger than the one with $4d_{3z^2-r^2}$ orbital at a distance of 4 a.u. Also a slower decay with distance is obtained for the 5s orbital, as it should be for delocalized orbitals.

Figure 2 shows the potentials V_{aa} defined by Eq. (5) as a function of the distance z, for the case of He on top of the Ag atom placed at $\vec{R} = 0$ and for (a) $q_{\parallel} = 0.1$ a.u., $z_a = 4$ a.u., (b) $q_{\parallel} = 0.1$ a.u., $z_a = 1$ a.u., (c) $q_{\parallel} = 0.6$ a.u., $z_a = 4$ a.u., and (d) $q_{\parallel} = 0.6$ a.u., $z_a = 1$ a.u. These values of the momentum transfer $q_{\parallel}$ are typical for large and short atom-surface distances, respectively. The exponential factor $e^{-q_{\parallel}|z-z'|}$ appearing in the matrix elements of Eq. (5) acts as a cutoff in momentum space: for large distances only small values of $q_{\parallel}$ are allowed while large values of $q_{\parallel}$ contribute to the Auger rate at short distances. Notice that, since orbitals $|\varphi_a\rangle$ and
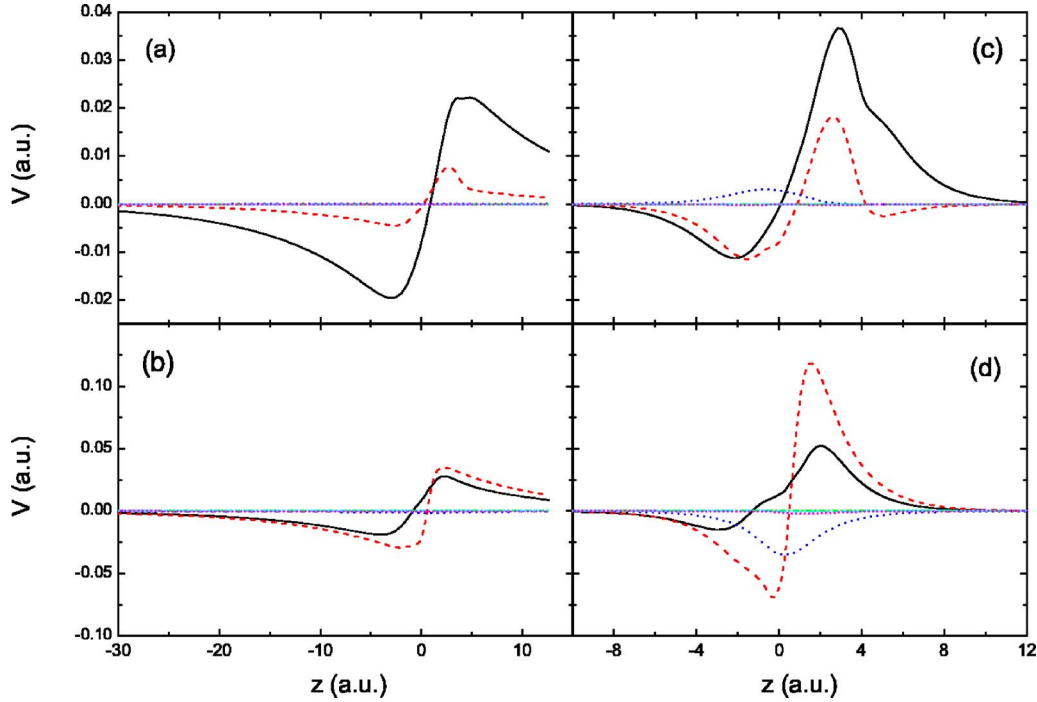
FIG. 2. (Color online) Potentials defined by Eq. (5) as a function of distance to the first atomic layer, for He on top of the Ag atom placed at $\vec{R}=0$, for (a) $q_\parallel=0.1$ a.u., $z_a=4$ a.u., (b) $q_\parallel=0.1$ a.u., $z_a=1$ a.u., (c) $q_\parallel=0.6$ a.u., $z_a=4$ a.u., and (d) $q_\parallel=0.6$ a.u., $z_a=1$ a.u. Solid line: $\alpha=5s$ orbital. Dashed line: $\alpha=4d_{3z^2-r^2}$ orbital. Dotted line: $\alpha=4d_{x^2-y^2}$ orbital.

$|\varphi_\alpha\rangle$ are orthonormal, the potentials $V_{\alpha a}(z)$ are dipolelike. For the small value of $q_\parallel$ in Figs. 2(a) and 2(b), the potentials $V_{\alpha a}(q_\parallel,z)$ behave, as a function of z, like the potentials of a dipole perpendicular to the surface. One can observe that the dipole moment is certainly proportional to the overlap integral, and the potentials of orbitals other than $5s$ or $4d_{3z^2-r^2}$ ones are negligibly small, as described above. In Figs. 2(c) and 2(d), $q_\parallel$ is of the order of q_F and the proportionality between dipole moment and overlap is not as good as in the previous case, as expected. It is remarkable that at the short distance of Fig. 2(d), the potential of the $4d_{3z^2-r^2}$ is much larger that the one of the $5s$ orbital and even the potential due to the $4d_{x^2-y^2}$ orbital is non-negligible. These results point towards the important role that d electrons are to play in the Auger neutralization rate of He on Ag at distances shorter than 2–3 a.u. as we will show in Sec. IV.

Finally, another important ingredient to understand the experimental results is provided by the calculation of the scattered ion trajectories. Since we deal with grazing scattering, we perform classical molecular dynamic simulations using the code KALYPSO (Ref. 44) in which Ziegler-Biersack-Littmark (ZBL) potentials are used. Lattice vibrations at room temperature are included in the code; atoms are assumed to vibrate independently with amplitudes obtained for surface Debye temperatures of 142 K and 173 K, for normal and parallel motion, respectively. Out of all our simulated trajectories, we select those that reach our "small detector" defined by an aperture of $\Delta\theta=0.1°$ and $\Delta\psi=1.0°$ with respect to the specular direction, θ being the scattering angle and ψ the azimuthal angle. These values correspond to the angular acceptance of the experimental detector. Then, for each trajectory, we calculate the ion survival probability as

$$P_i = \exp\left\{-\int_{t_i}^{t_f}\frac{dt}{\tau_A}[\vec{R_a}(t)]\right\}, \quad (11)$$

t_i and t_f being initial and final times in the simulation. The ion fraction, to be compared with the experiment, is calculated as $I=\frac{\Sigma_i P_i}{N}$, where N is the total number of trajectories that reach the detector. Inclusion of thermal vibrations is very important for obtaining N (Refs. 12 and 28) and thus the theoretical ion fraction. A source of uncertainly in the calculation of the ion trajectories is set by the acceleration and deceleration of the ion as a consequence of its interaction with the metal surface, which for large distances is given by the image potential, but for short distances has to be calculated in an elaborate way. To see how robust our results are we have performed simulations for two conditions: (i) we assume there is no change in energy due to the ion-surface interaction and (ii) we increase the ion perpendicular energy by 2.0 eV, which is the typical value of the energy gain of He$^+$ on a variety of solid surfaces. This leads to an increase in the angle of incidence of the simulated trajectories with respect to the experimental value of 3.5°. All the results we will present in Sec. IV are obtained using approximation (ii), and we have checked that the use of (i) introduces changes of 35% in the worst case. Moreover, the analysis of rainbow effects in the scattering of neutral He along the [110] direction of Al(111) and Ag(111) surfaces performed in Ref. 45 seems to show that the ZBL potential is too repulsive. However, this analysis is based on an average of pair potentials over atomic strings and neglects lattice vibrations. In our analysis using molecular dynamics, we find a very important effect of lattice vibrations and, moreover, we have the uncer-

tainty of the effect of the image-charge acceleration. Therefore, we prefer to use a "universal" potential (such as the ZBL potential) without adjustable parameters.

III. EXPERIMENTS

Our experiments focused on the determination of Auger neutralization probabilities in He$^+$ scattering on Ag(110) and Ag(111) surfaces, for various azimuthal orientations of the target in order to get a complete picture as a function of the kind of trajectory of the scattered ions. The azimuthal angular dependence of Auger neutralization on Ag(110) and a comparison of neutralization for a random scattering direction on Ag(110) and Ag(111) were presented earlier and details may be found in Refs. [12]–[14]. Here we present new experimental results for the azimuth-dependent neutralization on Ag(111) and previously unpublished results for Ag(110).[14] The experiments were performed on the ultrahigh-vacuum setup described in detail elsewhere.[46] He$^+$ ion fraction measurements were made for a fixed scattering angle of 7° using a position-sensitive channel plate detector equipped with three discrete anodes, which counts simultaneously particles of different charge states. The positive ion fractions are defined as the ratio of the scattered He$^+$ flux to the total scattered flux into a given angle with respect to the surface plane. Measurements were performed for specular scattering conditions. The incidence angle setting was thus 3.5°, set with an accuracy of ±0.1°. The Ag surface preparation included multiple cycles of grazing incidence ion beam sputtering and annealing, and time-of-flight recoil spectroscopy was used to check for absence of contaminants like H, C, and O.[46] The crystal azimuthal setting is determined by measuring the scattered intensity of the ion beam in the forward direction during an azimuthal scan. This allows a precision better than 0.2°.

Figure 3(a) shows a sketch of the Ag(111) surface indicating the azimuthal angle definitions. Figure 3(b) shows the azimuthal scattering profile for He scattering on Ag(111) including ions and neutrals. One can observe characteristics dips for the main symmetry directions indicated in Fig. 3(a). In the following the angle definitions refer to this figure. Results of ion fraction measurements will be shown later in the next section and compared with theory.

IV. RESULTS

A. Ag(110) surface

Figure 4 shows different contributions to the Auger neutralization rate as a function of the distance to the first atomic layer, assuming that He approaches the surface on top of a Ag atom. The comparison of the contribution of the atom on top of He (dots) with that of the rest of atoms (diamonds) shows that a He$^+$ ion will be neutralized by electrons of this atom of Ag at close distances. This is completely different to what we found for He$^+$ neutralization on Al(110) in Ref. [30] in which case even atoms in the second atomic layer gave a contribution as large as that of the Al atom on top of He. The difference between Ag and Al resides in the contribution of d
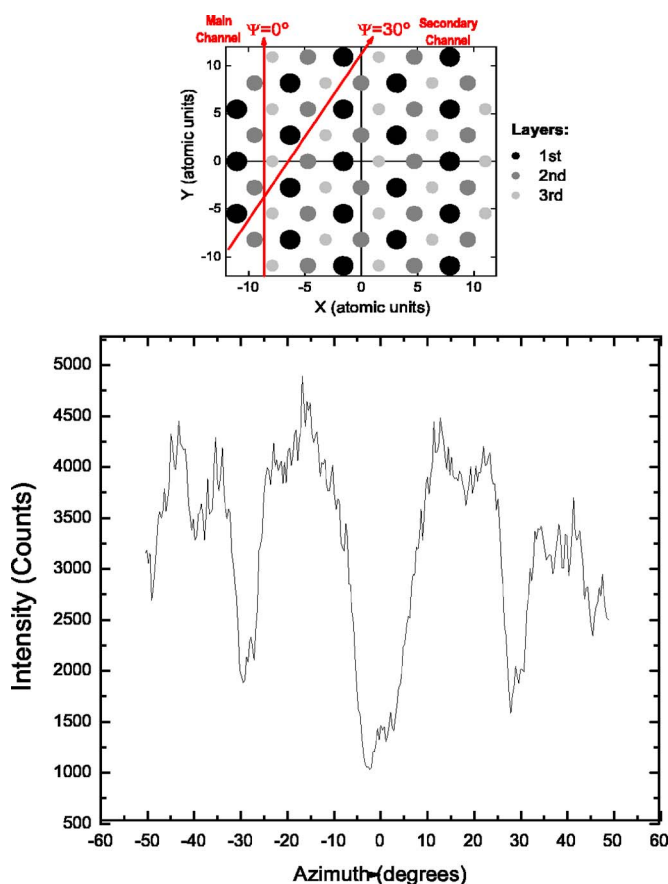

FIG. 3. (Color online) (a) Sketch of the Ag(111) surface indicating the azimuthal angle definitions. (b) The intensity of the azimuthal scattering profile for He scattering on Ag(111) including ions and neutrals.

electrons. Figure 4 also shows separately the contributions of s and d electrons. As we anticipated, s electrons make the most important contribution at distances larger than 4 a.u. but for distances shorter than 2 a.u. the Auger neutralization rate is practically given by the contribution of the d electrons: their overlap with He is as large as that of s electrons, and they are more numerous. Finally at very short distances (smaller than 1 a.u.), the effect of d electrons tends to decrease again, in the same way as their overlap with He does.[47] It can be appreciated in Fig. 4 that the total Auger rate (represented by squares in the figure) is almost identical to the sum of the individual contributions of s and d electrons. This is because crossed terms like $\alpha = s$, $\alpha' = d$ appearing in the sums of Eq. (4) are weighted by the crossed densities of states $\rho_{s\vec{R};d\vec{R'}}(\epsilon)$. These present large oscillations as a function of the electron energy ϵ that finally lead to cancellation of the corresponding contribution.

Figure 5 shows the dependence with the distance perpendicular to the surface of the Auger rate assuming He to be at the following symmetry positions with respect to the unit cell of the (110) surface: on top, center hollow and the two bridge positions. Bridge 1 is at a distance 2.73 a.u. and bridge 2 at 3.87 a.u. from a Ag atom, in the middle of the short and long sides of the surface unit cell, respectively. One can appreciate how the Auger rate is independent of lateral position
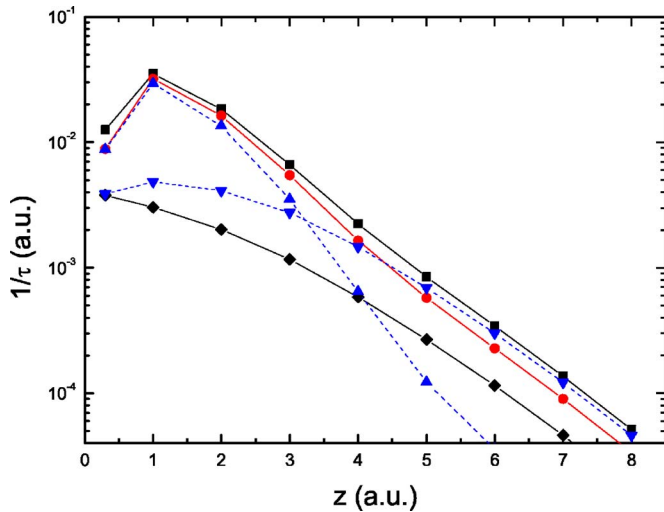
FIG. 4. (Color online) The Auger neutralization rate of He$^+$ approaching the Ag(110) surface on top of an Ag atom is plotted as a function of the distance to the first atomic layer. Squares, solid line: total Auger rate. Down triangles, dashed line: contribution of *s* electrons. Up triangles, dashed line: contribution of *d* electrons. Dots, solid line: contribution of Ag atom on top of He, only. Diamonds, solid line: contribution of the rest of Ag atoms.

for distances to the surface larger than 4 a.u. because it is given by the contribution of the extended *s* electrons of many atoms. However, for shorter distances, *d* electrons come into play. Their contribution to the Auger rate depends on the relative distance to He and the number of neighbors. Therefore the Auger rate shows a non-negligible dependence on lateral position at close distances. The corrugation dependence of the Auger rate is more clearly shown in Fig. 6, where we have plotted it as a function of parallel distance for a fixed perpendicular distance of $z_a = 2$ a.u. and for three values of the azimuth. The thick solid line is for the [110] direction, the dash-dotted line for the [111] direction, and the
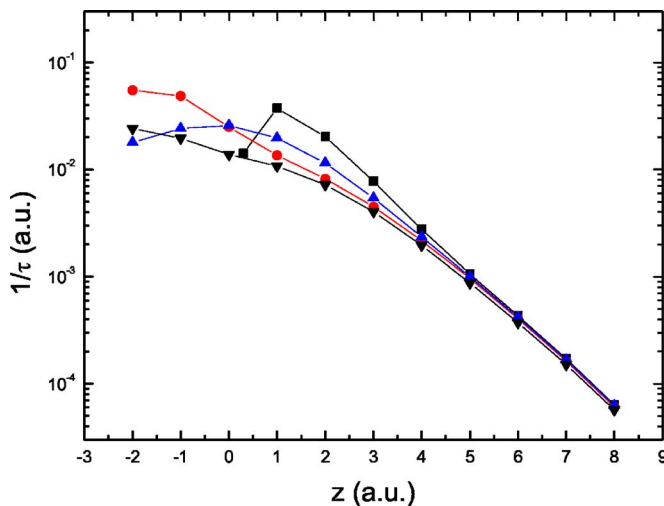

FIG. 5. (Color online) The Auger neutralization rate of He$^+$ approaching perpendicularly the Ag(110) surface at the lateral positions on top (squares), center hollow (dots), bridge 1 (up triangles) and bridge 2 (down triangles).
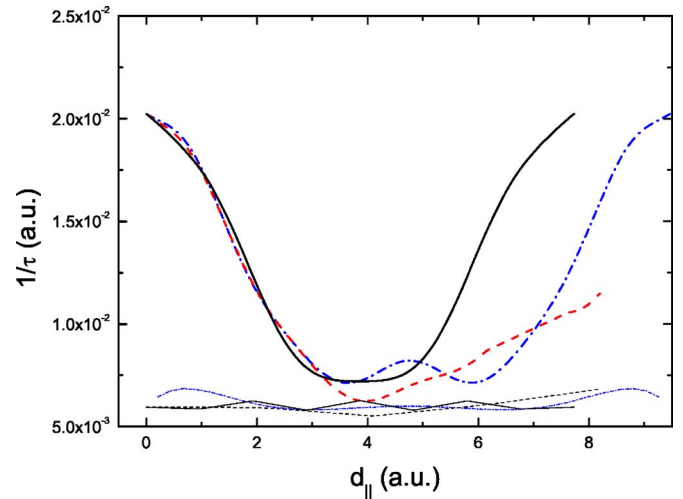

FIG. 6. (Color online) The Auger neutralization rate of He on Ag(110) as a function of parallel distance to a Ag atom for $z_a = 2$ a.u. when we move along the [110] direction (solid line), the [111] direction (dash-dotted line), and a "random" direction of 19.5° with respect to the [110] direction (dashed line). For the three cases we plot the contribution of *s* and *d* electrons (thick lines) and the contribution of *s* electrons only (thin lines).

dashed line for a direction of 19.5° with respect to the [110] direction ("random" direction). Common to the three directions is the strong decrease of the rate with parallel distance from the Ag atom at $d_\parallel = 0$. The contributions of *s* electrons are also shown in the figure as thin lines. They are nearly independent of direction along the lattice and of parallel distance because *s* electrons are delocalized and many atoms contribute. In contrast, the localization of *d* electrons makes their contribution to be important only for interatomic distances of Ag-He smaller than 3–4 a.u. The small maximum at a lateral distance of ∼5 a.u. for the [111] direction is due to the contribution of the *d* electrons of the Ag atom of the second atomic layer. For the random direction the Auger rate first decreases with distance as He moves away from a Ag atom and then increases again towards the bridge 1 position.

As we explained in Sec. II, the other important ingredient of our calculation is provided by the scattered trajectories. Except for the [110] and [100] symmetry directions, where a large number of particles penetrate the first atomic layer, the scattered trajectories stay above the surface. The apexes of these trajectories present a nearly Gaussian distribution, the maximum of which we identify with the distance of closest approach. For a random direction, the values of this distance are in the range of 0.7–2.3 a.u. for the incident energies of 4–0.5 keV used in the present experiments. Then the trajectories reach to distances where the contribution of *d* electrons to the total Auger neutralization rate is important, at all incident energies.

In a previous work[31] we presented a comparison of our theory with the experimental ion fraction as a function of azimuth for incident energies of 1 keV and 2 keV. In Fig. 7 we show the same comparison for (a) 3 keV and (b) 4 keV. All the experimental data are for a fixed incidence angle of 3.5° with respect to the surface. The good agreement between theory and experiment already shown in Fig. 3 of Ref.
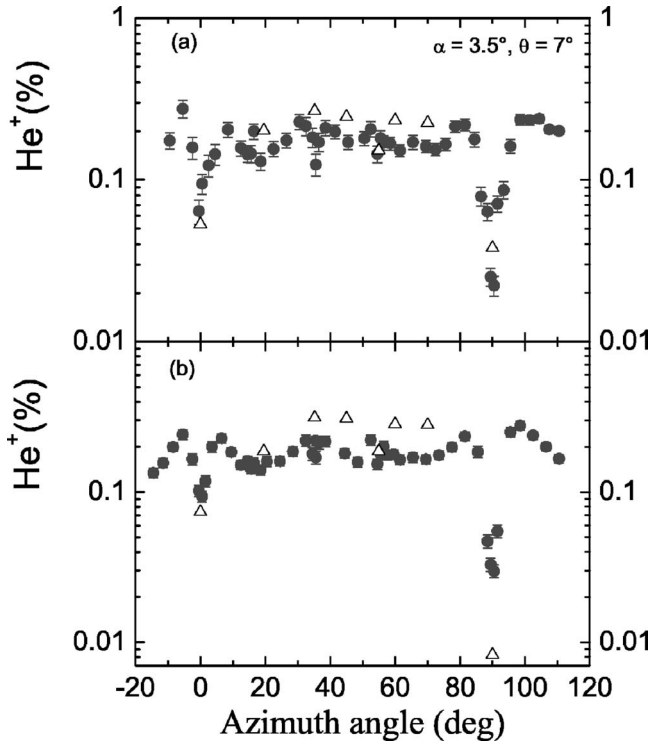
FIG. 7. The ion fraction versus azimuthal angle for He$^+$ of (a) 3 keV and (b) 4 keV of incident energy on the Ag(110) surface. The experimental results (dots) are compared with our theoretical results (triangles).

31 for small incident energies is kept for the higher kinetic energies as well. The deep minima in ion fraction at 0° and 90° are due to the fact that many particles penetrate the first atomic layer and get completely neutralized. Out of these symmetry directions the scattered trajectories stay above the surface. The weak dependence of the ion fraction with azimuthal angle for random directions can be understood by looking to the values of the Auger rates shown in Fig. 6. At grazing conditions the trajectory lengths are large, of the order of 10 unit cells, but for random directions the He$^+$ ion passes seldom on top of a Ag atom. Therefore most of the time the value of the Auger neutralization rate it experiences is that of the flattest part of Fig. 6, which do not change much with azimuth. The largest differences between theory and experiment are obtained at the highest energy of 4 keV. We think this is due to the worse statistics of useful trajectories we get when we increase the incident energy, because our LCAO theory should be more accurate for the shorter distances between ion and surface attained at these energies. In the simulation, for a given number of incident trajectories, the number of them that reach the "detector" decreases quickly with incident energy. Therefore, to have reliable results, we have to increase the number of simulated trajectories with the consequent increase of computer time. In our experience, differences in ion fraction with azimuth tend to wash out when we improve the calculation along this line and also the theory gets closer to the experiment. Nevertheless, the results already presented for the (110) surface together with the results for the (111) surface we will present next clearly show the importance of d electrons and the
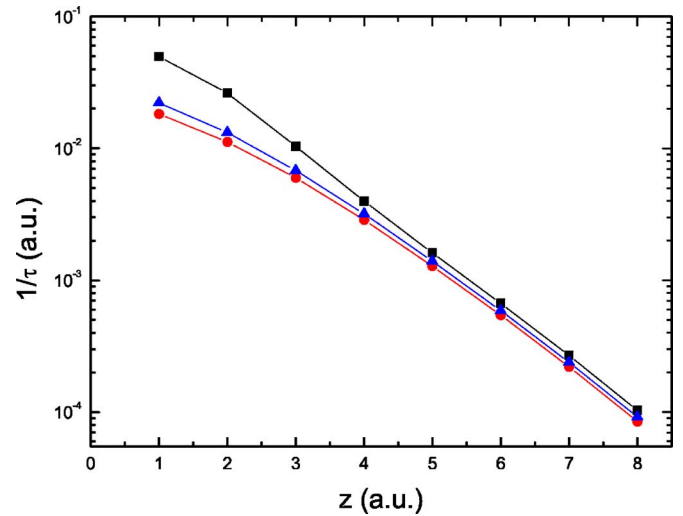

FIG. 8. (Color online) The Auger neutralization rate of He$^+$ approaching perpendicularly the Ag(111) surface at the lateral positions on top (squares), center hollow (dots), and bridge (up triangles).

accuracy of our approximation for describing Auger neutralization.

B. Ag(111) surface

All the characteristics already discussed for the (110) surface apply to the (111) surface as well. In Fig. 8 we plot the Auger neutralization rate versus distance perpendicular to the first atomic layer for three lateral positions: on top, center hollow (the two nonequivalent center hollow positions are virtually indistinguishable), and bridge. Again, the Auger rate is sensitive to lateral position only for perpendicular distances shorter than 4 a.u., when the contribution of d electrons is not negligible. Also, when the rate is plotted versus parallel distance, we obtain a pattern similar to the one shown in Fig. 6 for the (110) surface. However, the effects of lateral corrugation are less pronounced than for the (110) surface due to the closer packing of the (111) surface.

Figure 9 shows results for the surviving ion fraction for He$^+$ scattering on Ag(111). As may be seen this is very small being about 0.04% for random scattering directions. A fairly strong variation in the ion fraction is only observed near the 0° direction around which a significantly higher fraction of surviving ions may be noted. The results of our theoretical calculation are represented by open dots in this figure. At 0° we find two groups of trajectories, one group corresponding to particles traveling far from the surface above atomic chains and the other group traveling very close to the surface in between two atomic chains. This is similar to what we found for the (110) surface at symmetry directions, and we also find a minimum of the ion fraction. This situation changes very rapidly with azimuth, and at an angle of 4° we only find one kind of trajectories and consequently an increase in the ion fraction. For higher values of the azimuth, the ion fraction tends to decrease as the secondary channel shown in Fig. 3(a) is approached. It is remarkable that the theory reproduces the experimental trend and the magnitude
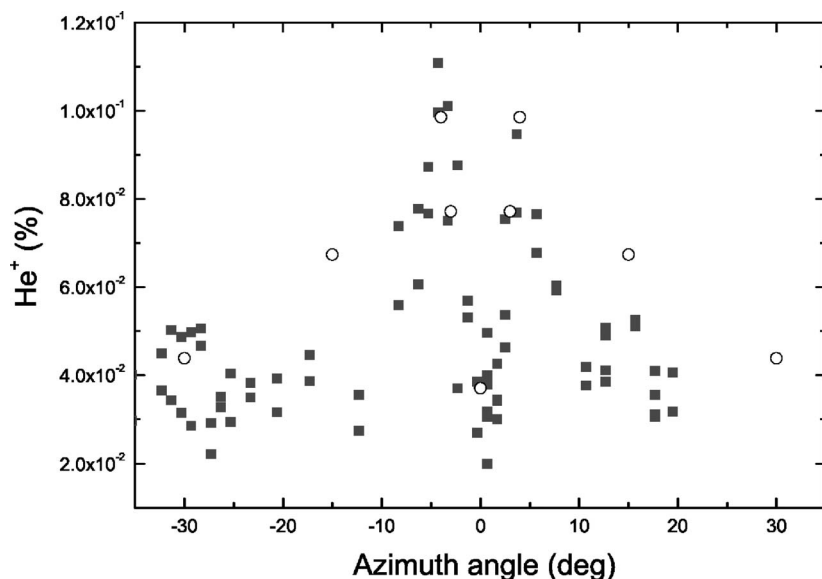
FIG. 9. The ion fraction versus azimuthal angle for He$^+$ incident on the Ag(111) surface with 4 keV of energy. The experimental results (squares) are compared with the theoretical results of our calculations (open dots).

of the ion fraction as well, which shows the accuracy of the present calculation.

V. CONCLUSIONS

In this article we have analyzed the problem of Auger neutralization of He$^+$ scattered off Ag(110) and Ag(111) surfaces, including the previously ignored role of d electrons and focusing on azimuthal effects. We have shown theoretically that the matrix elements for the Auger transition are approximately proportional to the overlap integral between the atomic orbitals of the metal and the ion. This allows us to infer the relative role played by different types of atomic orbitals in the neutralization process. The theory shows that the contribution of d electrons to the Auger rate starts to be of increasing importance for interatomic distances shorter than ~ 3 a.u. Thus, while the contribution of s electrons basically only depends on the distance perpendicular to the surface, the contribution of d electrons depends on the lateral position of He with respect to the surface unit cell, producing strongly corrugated values of the total Auger neutralization rate. When comparing our calculated Auger rate for the (111) and (110) surfaces, we find larger values and less corrugation for the former surface than for the latter, as it should be, since the fcc (111) surface is the closest-packed one. Our position-dependent Auger rate is used along with molecular dynamics simulation of scattered trajectories, yielding a calculated ion fraction which is compared to the experiment. The excellent agreement between theory and experiment we find for many values of the azimuth and ion incident energies and for both Ag(110) and Ag(111) surfaces, without adjustable parameters, shows the important role played by localized electrons in Auger neutralization processes even under grazing scattering conditions.

*Email address: diego.valdes@uam.es

[1] J. D. White, J. Chen, D. Matsiev, D. J. Auerbach, and A. M. Wodtke, Nature (London) **433**, 503 (2005).

[2] J. D. White, J. Chen, D. Matsiev, D. J. Auerbach, and A. M. Wodtke, J. Chem. Phys. **124**, 064702 (2006).

[3] J. J. C. Geerlings and J. Los, Phys. Rep. **190**, 133 (1990).

[4] A. G. Borisov, D. Teillet-Billy, and J. P. Gauyacq, Phys. Rev. Lett. **68**, 2842 (1992).

[5] M. Maazouz, A. G. Borisov, V. A. Esaulov, J. P. Gauyacq, L. Guillemot, S. Lacombe, and D. Teillet-Billy, Phys. Rev. B **55**, 13869 (1996).

[6] P. Nordlander and J. C. Tully, Phys. Rev. Lett. **61**, 990 (1988); Phys. Rev. B **42**, 5564 (1990).

[7] J. Merino, N. Lorente, P. Pou, and F. Flores, Phys. Rev. B **54**, 10959 (1996).

[8] P. G. Bolcatto, E. C. Goldberg, and M. C. G. Passeggi, Phys. Rev. A **50**, 4643 (1994).

[9] N. P. Wang, Evelina A. García, R. Monreal, F. Flores, E. C. Goldberg, H. H. Brongersma, and P. Bauer, Phys. Rev. A **64**, 012901 (2001).

[10] K. Niedfeldt, E. A. Carter, and P. Nordlander, J. Chem. Phys. **121**, 3751 (2004).

[11] A. R. Canario, A. G. Borisov, J. P. Gauyacq, and V. A. Esaulov, Phys. Rev. B **71**, 121401(R) (2005).

[12] Yu. Bandurin, V. A. Esaulov, L. Guillemot, and R. C. Monreal, Phys. Rev. Lett. **92**, 017601 (2004).

[13] R. C. Monreal, L. Guillemot, and V. A. Esaulov, J. Phys.: Condens. Matter **15**, 1165 (2003).

[14] Yu. Bandurin, V. A. Esaulov, L. Guillemot, and R. C. Monreal, Phys. Status Solidi B **241**, 2367 (2004).

[15] S. Wethekam, A. Mertens, and H. Winter, Phys. Rev. Lett. **90**, 037602 (2003).

[16] S. Wethekam and H. Winter, Surf. Sci. **596**, 319 (2005).

[17] S. Wethekam and H. Winter, Phys. Rev. Lett. **96**, 207601 (2006).

[18] T. Fonden and A. Zwartkruis, Phys. Rev. B **48**, 15603 (1993).

[19] H. Jouin, F. A. Gutierrez, and C. Harel, Phys. Rev. A **63**, 052901 (2001).

[20] R. Monreal and N. Lorente, Phys. Rev. B **52**, 4760 (1995).

[21] N. Lorente and R. Monreal, Phys. Rev. B **53**, 9622 (1996); Surf. Sci. **370**, 324 (1997).

[22] M. A. Cazalilla, N. Lorente, R. D. Muiño, J.-P. Gauyacq, D. Teillet-Billy, and P. M. Echenique, Phys. Rev. B **58**, 13991 (1998).

[23] W. More, J. Merino, R. Monreal, P. Pou, and F. Flores, Phys. Rev. B **58**, 7385 (1998).

[24] N. D. Lang and W. Kohn, Phys. Rev. B **1**, 4555 (1970).

[25] H. D. Hagstrum and G. E. Becker, Phys. Rev. **159**, 572 (1967).

[26] M. Canepa, P. Cantini, L. Mattera, S. Terreni, and F. Valdenazzi, Phys. Scr. **T41**, 226 (1992).

[27] L. Pasquali, M. C. Sapet, E. M. Staicu-Casagrande, P. Cortona, V. A. Esaulov, S. Nannarone, M. Canepa, S. Terreni, and L. Mattera, Nucl. Instrum. Methods Phys. Res. B **212**, 274 (2003).

[28] A. Narmann, K. Schmidt, W. Heiland, R. Monreal, F. Flores, and P. M. Echenique, Nucl. Instrum. Methods Phys. Res. B **48**, 378 (1990).

[29] A. Narmann, W. Heiland, R. Monreal, F. Flores, and P. M. Echenique, Phys. Rev. B **44**, 2003 (1991).

[30] Diego Valdés, E. C. Goldberg, J. M. Blanco, and R. C. Monreal, Phys. Rev. B **71**, 245417 (2005).

[31] Diego Valdés, J. M. Blanco, V. A. Esaulov, and R. C. Monreal, Phys. Rev. Lett. **97**, 047601 (2006).

[32] Per-Olov Löwdin, J. Chem. Phys. **18**, 365 (1950).

[33] S. Huzinaga, J. Chem. Phys. **42**, 1293 (1965).

[34] H. Vázquez, R. Oszwaldowski, P. Pou, J. Ortega, R. Perez, F. Flores, and A. Kahn, Europhys. Lett. **65**, 802 (2004).

[35] M. A. Basanta, Y. J. Dappe, J. Ortega, and F. Flores, Europhys. Lett. **70**, 355 (2005).

[36] F. J. García-Vidal, A. Martin-Rodero, F. Flores, J. Ortega, and R. Perez, Phys. Rev. B **44**, 11412 (1991).

[37] E. C. Goldberg, A. Martín-Rodero, R. Monreal, and F. Flores, Phys. Rev. B **39**, 5684 (1989).

[38] Pavel Jelinek, Hao Wang, James P. Lewis, Otto F. Sankey, and J. Ortega, Phys. Rev. B **71**, 235101 (2005).

[39] H. Ishida and A. Liebsch, Phys. Rev. B **66**, 155413 (2002).

[40] C. López-Bastidas, A. Liebsch, and W. L. Mochán, Phys. Rev. B **63**, 165407 (2001).

[41] Jesús Tarriba and W. L. Mochán, Phys. Rev. B **46**, 12902 (1992).

[42] A. García-Lekue, J. M. Pitarke, E. V. Chulkov, A. Liebsch, and P. M. Echenique, Phys. Rev. Lett. **89**, 096401 (2002).

[43] H. Ehrenreich and H. R. Philipp, Phys. Rev. **128**, 1622 (1962).

[44] M. A. Karolewski, Nucl. Instrum. Methods Phys. Res. B **230**, 402 (2005).

[45] A. Schüller, G. Adamov, S. Wethekam, K. Maass, A. Mertens, and H. Winter, Phys. Rev. A **69**, 050901(R) (2004).

[46] V. Esaulov, L. Guillemot, O. Grizzi, M. Huels, S. Lacombe, and Vu Ngoc Tuan, Rev. Sci. Instrum. **67**, 1 (1996).

[47] The values of $\frac{1}{\tau}$ at $z=0$ plotted in Fig. 1(a) of Ref. [31] were incorrect. We have checked that the error does not affect the results of Ref. [31] because scattered particles never get that close to the surface.